Optics Letters

Yb:fiber laser-based, spectrally coherent and efficient generation of femtosecond 1.3-μm pulses from a fiber with two zero-dispersion wavelengths

Yuhong Yao,* Govind P. Agrawal, and Wayne H. Knox

The Institute of Optics, University of Rochester, Rochester, New York 14627-0186, USA
**Corresponding author: yuhongopt@gmail.com*

Received 12 June 2015; revised 9 July 2015; accepted 13 July 2015; posted 14 July 2015 (Doc. ID 242913); published 29 July 2015

We report, to the best of our knowledge, the first experimental characterization of spectral coherence properties of wavelength conversion inside photonic crystal fibers with two zero-dispersion wavelengths (TZDWs) and demonstrate a low-noise femtosecond 1.3-μm source employing the TZDW fiber and a 1.3-W, 240-fs Yb:fiber amplifier as the seeding source. Theoretical investigation shows that pulse evolution in our TZDW fiber source is dominated by parametric amplification seeded by self-phase modulation broadening which efficiently converts the pump energy into two new wavelength bands in a deterministic manner, leading to low noise and coherent excitation of femtosecond pulses tunable in the 1.3-μm spectral region, with up to 3 nJ of pulse energy at 32% of conversion efficiency.

OCIS codes: (030.1640) Coherence; (140.7090) Ultrafast lasers; (320.6629) Supercontinuum generation.

http://dx.doi.org/10.1364/OL.40.003631

Fiber supercontinuum sources employing nonlinear frequency conversion in photonic crystal fibers (PCFs) have been studied extensively in the past decade, leading to a number of novel applications [1]. While expanding the supercontinuum spectral bandwidth was the goal of initial studies, increasing efforts have been carried out on isolating individual nonlinear processes such as soliton self-frequency shift (SSFS) [2,3], Cherenkov radiation [4,5], and four-wave mixing [6] for efficient frequency conversion to specific wavelengths of interests. With advancements in Yb:fiber laser technologies, such approaches become promising solutions toward all-fiber integration of ultrafast sources operating at wavelengths traditionally only accessible by solid-state lasers [3,5]. Using conventional PCFs with a single zero-dispersion wavelength (ZDW), pulse energy of the frequency converted source is usually constrained, since a *broadband* supercontinuum can easily be excited beyond certain pump energies. Moreover, the occurrence of nondeterministic processes such as soliton fission and modulation instability (MI), which take place in the fiber's anomalous dispersion region (ADR), can lead to severe coherence degradation and pulse-to-pulse fluctuations due to amplification of pump shot noise, unless careful controls of launching parameters (i.e., low soliton order, short pulse widths) are made [7,8]. Employing a PCF with all-normal dispersion would solve the decoherence problem; however, its spectral broadening is manifest as a flat-top continuum around the pump wavelength, which is less efficient for conversion to targeted wavelengths.

In contrast to these two fiber types, PCF with two-ZDWs (TZDWs) offers a unique route to efficient energy transfer from the pump wavelength to two localized spectral regions *beyond* either side of the ZDWs [9]. In previous work, we have employed an Yb:fiber amplifier to excite an intense Stokes pulse around ∼1.26 μm from a TZDW PCF for mid-IR difference-frequency generation [10,11] and speckle-free RGB generation [12]. The ∼1.3 μm region is an important optical window for deep-tissue imaging [13] that is traditionally accessed with Cr:forsterite lasers. We believe that integration of the Yb:fiber laser and the TZDW PCF could lead to an all-fiber ultrafast source as an alternative to solid-state lasers. For reliable stand-alone operation, intensity stability and spectral coherence are essential. Since the pump wavelength lies in the ADR of fiber, it is necessary to investigate whether the TZDW fiber output is susceptible to decoherence and intensity instability with respect to variations in pump pulse parameters. Although TZDW continuum with low intensity noise was observed with a sub-100-fs Nd:Glass oscillator as the seeding source [14], no experimental investigation on its spectral coherence property has been reported to date, and it is not obvious if low-noise continuum generation can be accomplished with the 200–300-fs pulse pumping regime.

In this Letter, we investigate the nonlinear pulse evolution, coherence, and noise properties of the Stokes side emission generated in a commercially available TZDW PCF excited by a

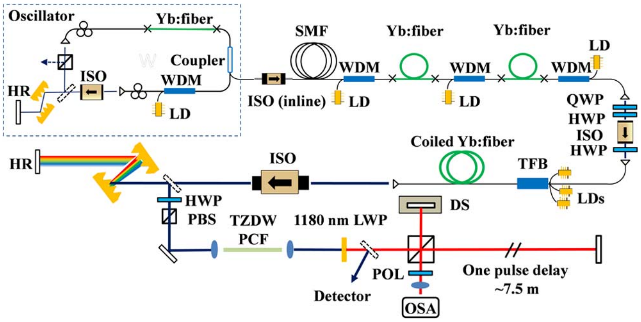

Fig. 1. Experimental setup of the TZDW fiber source and subsequent coherence measurement system. HR, high reflector; ISO, isolator; WDM, wavelength division multiplexer; LD, laser diode; SMF, single-mode fiber; QWP, quarter wave plate; HWP, half-wave plate; TFB, taper fiber bundle; DS, delay stage; PBS, polarizing beam splitter; LWP, long-wave pass filter; POL, polarizer.

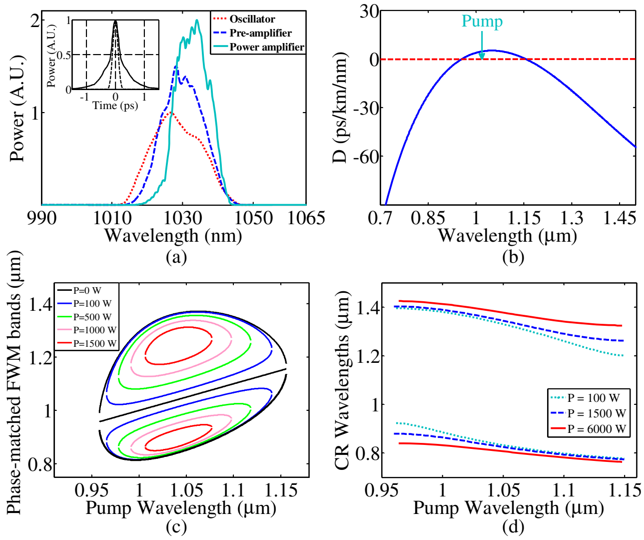

Fig. 2. (a) Measured output spectra of the oscillator, pre-amplifier, and power amplifier (spectral intensity normalized to 1, 1.5, and 2, respectively). Inset: measured autocorrelation trace (solid line) of the compressed MOPA output and calculated autocorrelation trace of the transform-limited pulse (dotted line). (b) Calculated dispersion profile of the TZDW PCF; the dotted line indicates zero dispersion wavelengths. (c) Power-dependent phase-matched four-wave mixing bands of the PCF. (d) Phase-matched Cherenkov radiation bands of the PCF.

1.3-W, 240-fs Yb:fiber master-oscillator-power-amplifier (MOPA). We confirm that pulse evolution in our TZDW fiber source is dominated by parametric amplification seeded by self-phase modulation (SPM) broadening, which efficiently transfers the pump energy into the Stokes band in a deterministic manner, leading to low noise and coherent excitation of femtosecond Stokes pulses with peak wavelength tunable between 1200 and 1285 nm, with up to 3 nJ of pulse energy at 32% of conversion efficiency.

Figure 1 illustrates the experimental set-up consisting of the TZDW fiber source and the measurement system. The pump source is a custom-built Yb:fiber MOPA that is seeded by an Yb:fiber oscillator passively mode-locked via nonlinear polarization evolution [15]. The oscillator produces 39.6-MHz, 20-mW average power pulses centered at 1027 nm [red dotted line in Fig. 2(a)]. With its pulse width stretched to ~18 ps within 20 m of single-mode fiber (Lucent 980), the oscillator output is amplified to ~300 mW by a two-stage pre-amplifier whose center wavelength is shifted to 1030 nm due to spectral filtering of the WDMs [blue dashed line in Fig. 2(a)]. Further amplification is achieved by a power amplifier consisting of ~3 m double-clad Yb:fiber (Nufern PLMA-YDF-15/130) pumped by three 3-W multimode laser diodes that are combined with the pre-amplifier output by a tapered fiber bundle (TFB). Measured chirped pulses' power following the double-clad gain fiber is as high as 4.8 W. By properly adjusting the distance between a diffraction grating pair (600 l/mm), we achieve compressed pulses with a measured autocorrelation width of 330 fs (FWHM), shown as the solid curve in the inset of Fig. 2(a). In the same figure, we plot the autocorrelation trace of the transform-limited pulse calculated from the amplifier spectrum [green line in Fig. 2(a)], showing an FWHM width of 260 fs. The final MOPA output has 1.3 W of average power, 1035 nm of center wavelength, and its pulse width is calculated to be 240 fs assuming a Gaussian pulse shape.

The TZDW fiber we use is 12 cm of 1050-NL-2 that is commercially available from NKT Photonics. The dispersion profile of our sample is determined by measuring its average pitch and air-hole sizes from scanning electron microscopy and calculated using a finite-difference frequency-domain (FDFD) algorithm [16]. The PCF has two closely spaced ZDWs located at 956 and 1155 nm, as is shown in Fig. 2(b). The negative dispersion slope above 1.06 μm leads to two sets of FWM bands providing parametric gain for wavelengths both inside/outside of the fiber ZDWs as well as dual-phase-matched bands for Cherenkov radiation (CR) that are further away from the fiber ZDWs.

The properties of the TZDW fibers have been comprehensively studied in [9] wherein the nonlinear mechanism was found to be SPM broadening followed by degenerate FWM. The role of FWM was questioned in [17], and it was believed that CR may also contribute to spectral broadening beyond the ZDWs [17,18]. For PCFs with relatively wider ZDW spacing, SSFS followed by CR becomes dominant over the spectral broadening [19,20]. To confirm the pulse evolution dynamics of our TZDW fiber source, we model its nonlinear pulse evolution with a rigorous split-step Fourier transform algorithm [21] and plot the numerically simulated spectrograms according to Eq. (1), assuming a square-gate pulse of ~100 fs duration. Figure 3 shows the sliced spectrograms of a 240-fs Gaussian pulse with 15-kW peak power (150 mW average power) propagating in 150 mm of TZDW PCF:

$$S(\omega, t) = \left| \int_{-\infty}^{\infty} E(\tau) g(\tau - t) \exp(i\omega\tau) \mathrm{d}\tau \right|^2. \quad (1)$$

It can be seen from Fig. 3(a) that during the first 45 mm of propagation, SPM dominates pulse's spectral broadening, with its leading edge experiencing red-shift and the trailing edge experiencing blue-shift. As the spectral broadening continues, the outer SPM peaks extend into the FWM gain bands inside

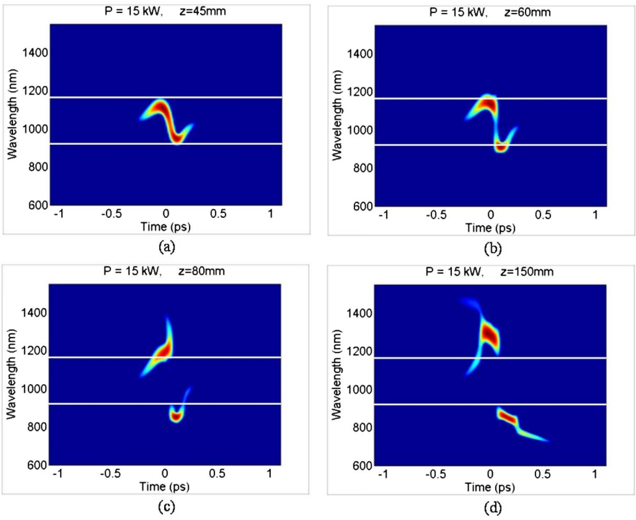

Fig. 3. Simulated spectrograms after propagation of (a) 45 mm, (b) 60 mm, (c) 80 mm, (d) 150 mm in the TZDW PCF for a 240-fs Gaussian input pulse at 1035 nm with 15 kW of peak power.

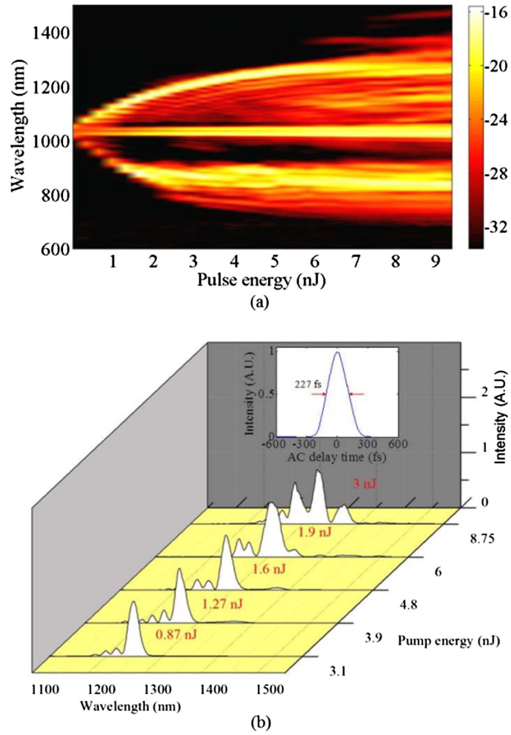

Fig. 4. (a) Measured TZDW PCF spectra (log scale) as a function of pump pulse energy. (b) Measured spectra (linear scale) and pulse energies of the filtered Stokes pulses as a function of pump energy. Inset: autocorrelation trace of the 1260-nm Stokes pulse.

the two fiber ZDWs, which provide the seeding power for parametric amplification and start to transfer power from the pump, as can be seen from Fig. 3(b). This in turn provides the seeding power at wavelengths outside the ZDWs that eventually deplete the residual power within the fiber ADR [Fig. 3(c)]. In contrast to MI, the seeded parametric amplification takes place in a fast, efficient, and deterministic manner and is expected to be spectrally coherent. The dual separated peaks continue to shift outward and eventually stabilize at around ~850 and ~1300 nm. Further propagation leads to pulse chirping within the normal dispersion region (NDR). It is at this stage that the accumulation of dispersive waves starts to show up [low intensity side-bands in Fig. 3(d)], which is characterized by their spreads in the temporal domain.

To compare with the simulation results, we couple the MOPA output into the TZDW PCF, and we use a PBS/HWP pair to control the amount of power for fiber coupling. Figure 4(a) records the PCF output spectra as a function of input pulse energy; the two localized continua on either side of the fiber ZDWs are clearly observed, and their spectral positions become fixed at ~850 and ~1300 nm at high pulse energies. The residual peak at the pump wavelength is attributed to the low-power pedestal of the amplifier output resulting from imperfect pulse compression of the MOPA system and is validated by re-simulating the nonlinear pulse evolution with a more realistic pulse shape. At modest pump energy, spectral red-shift of the Stokes band with increasing pump energy provides a tuning mechanism for the TZDW fiber source. To clearly observe its evolution, we use a long-wavelength-pass filter (DMLP-1180, Thorlabs) to filter out the spectral component above 1180 nm, showing that the Stokes band is manifest as a relatively narrow-band spectral peak tunable between 1200 and 1260 nm with a typical bandwidth of ~24 nm [Fig. 4(b)]. At 1260 nm peak wavelength, measured Stokes band energy is as high as 1.9 nJ, and the pulse preserves its ultrashort pulse width with measured autocorrelation width of 227 fs [shown in the inset of Fig. 4(b)]. This is due to the optimum PCF length that keeps the pulse evolution from accumulation of chirping in the fiber NDR. At higher input power, the Stokes band develops a more complex structure in the range of 1150–1350 nm. In both cases, efficient energy transfer from the pump wavelength is observed, with an average power conversion efficiency of 32.3% (photon efficiency ~39%).

First-order spectral coherence of the spectrum is characterized by the delay pulse cross-correlation method [22,23]. A Michelson interferometer with 7.5-m optical path difference (one cavity round trip time delay) is constructed where adjacent pulses from the two interferometer arms are combined at the output port, and the associated spectrograms are collected and analyzed with the OSA for calculation of the spectral coherence function [8], which is defined as

$$|g_{12}(\lambda, t_1 - t_2)| = \left|\sqrt{\frac{\langle E_1^*(\lambda, t_1)E_2(\lambda, t_2)\rangle}{\langle |E_1(\lambda, t_1)|^2\rangle\langle |E_2(\lambda, t_2)|^2\rangle}}\right|, \quad (2)$$

where $t_1 - t_2$ equals to the period of input pulses. A polarizer is implemented before the detector to ensure polarization overlap. The interferometer is tested with the pump pulses prior to the coherence measurement, showing capability of resolving 97% of fringe visibility. Typical spectral interferograms between consecutive Stokes pulses are shown in Fig. 5(a). Both spectra show strong fringes along the entire pulse bandwidth. Fringe visibilities are calculated and averaged across the interferograms to deduce the mean coherence. Figure 5(b) shows the mean

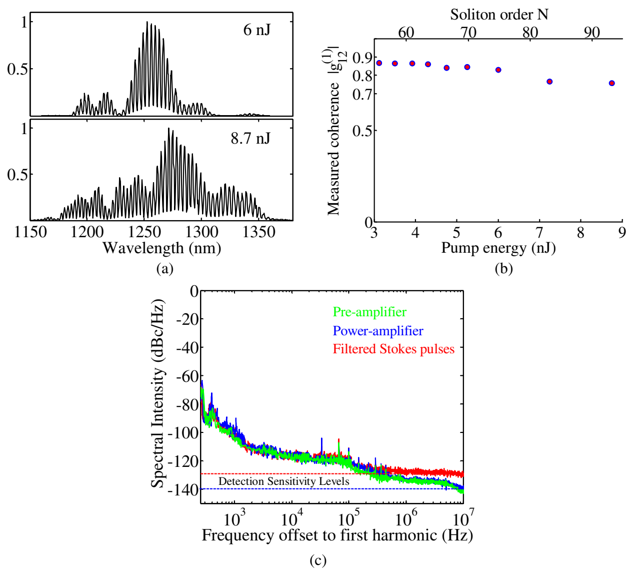

Fig. 5. (a) Measured spectral interferograms at 6 nJ and 8.7 nJ of pump pulse energy, respectively. (b) Measured average mutual coherence as a function of pump energy and its corresponding soliton order. (c) Measured RF noise spectra of the pre-amplifier output (green), Yb: fiber MOPA output (blue), and Stokes pulse (red) normalized to their carrier powers at first-harmonic frequency.

coherence at varying input pulse energy. Spectral coherence around 0.85 is observed for the modest power, narrow-band Stokes pulses, while fringe visibility drops for the broader Stokes band at highest pump energy. Still, spectral coherence $|g_{12}|$ higher than 0.76 is maintained at all cases while the soliton order N is increased to 90, confirming that the TZDW output is excited in a deterministic manner, with nonlinear mechanisms such as MI and soliton fission well suppressed, if not completely eliminated, along the pulse evolution within the fiber ADR.

The intensity noise is measured using a fast photodiode paired with an RF spectrum analyzer (Agilent 8564E). Figure 5(c) compares the RF noise spectrum of the filtered Stokes pulses with its peak at 1260 nm wavelength to those of the pre-amplifier and power amplifier outputs of the Yb:fiber MOPA. The noise measurement is performed at the first harmonic of the laser repetition rate (39.6 MHz) to provide calibrated measurements by normalizing the noise power to the carrier frequency power [14]. Detected carrier power was −10 dBm for the Stokes pulses and 2.3 dBm and 0 dBm, respectively, for the pre-amplifier and power-amplifier outputs. In contrast to supercontinuum generated in the single ZDW PCF, which exhibits white noise at high frequencies [7], RF spectrum of the Stokes pulses shows exponential decreasing of noise intensity at frequencies higher than 10 kHz, until hitting the detection sensitivity level that sets an upper limit of ∼5 dBc/Hz of escalation in noise spectral intensity from that of the Yb:fiber MOPA at 1–5-MHz frequency. Employing 240-fs seeding pulses at soliton order of ∼75, our result shows that the intensity stability of the TZDW output is robust against variations in pump pulse parameters and further confirms its deterministic nonlinear mechanism.

In conclusion, we have demonstrated a femtosecond 1.3 μm wavelength converter based on efficient, low-noise, and spectrally coherent Stokes band excitation from a TZDW PCF. Seeded by 240-fs pump pulses with soliton order $N > 50$, the Stokes band exhibits preservation of intensity stability and spectral coherence, which not only shows promising potential toward a robust all-fiber ultrafast source that can be helpful for applications such as biomedical deep-tissue imaging, but also attests to the stability of our reported approaches for mid-IR and RGB generation [10–12]. With the maturity in fiber laser technology, average power of the 1.3-μm source can be further scaled up with higher repetition rate source lasers [3,5,15].

Acknowledgment. The authors would like to thank Professor Goery Genty for helpful discussions on supercontinuum coherence.

REFERENCES

1. G. Genty, S. Coen, and J. M. Dudley, J. Opt. Soc. Am. B **24**, 1771 (2007).
2. N. Thanh Nam, K. Khanh, D. Churin, T. Ota, M. Miyawaki, and N. Peyghambarian, IEEE Photon. Technol. Lett. **25**, 1893 (2013).
3. J. Lim, H.-W. Chen, S. Xu, Z. Yang, G. Chang, and F. X. Kärtner, Opt. Lett. **39**, 2060 (2014).
4. H. Tu and S. A. Boppart, Opt. Express **17**, 9858 (2009).
5. H.-W. Chen, Z. Haider, J. Lim, S. Xu, Z. Yang, F. X. Kärtner, and G. Chang, Opt. Lett. **38**, 4927 (2013).
6. J. Cheng, M. E. V. Pedersen, K. Charan, K. Wang, C. Xu, L. Grüner-Nielsen, and D. Jakobsen, Appl. Phys. Lett. **101**, 161106 (2012).
7. K. L. Corwin, N. R. Newbury, J. M. Dudley, S. Coen, S. A. Diddams, K. Weber, and R. S. Windeler, Phys. Rev. Lett. **90**, 113904 (2003).
8. J. M. Dudley, G. Genty, and S. Coen, Rev. Mod. Phys. **78**, 1135 (2006).
9. K. M. Hilligsøe, T. Andersen, H. Paulsen, C. Nielsen, K. Mølmer, S. Keiding, R. Kristiansen, K. Hansen, and J. Larsen, Opt. Express **12**, 1045 (2004).
10. Y. Yao and W. H. Knox, Opt. Express **20**, 25275 (2012).
11. Y. Yao and W. H. Knox, Opt. Express **21**, 26612 (2013).
12. Y. Yao and W. H. Knox, Opt. Express **23**, 536 (2015).
13. D. Kobat, M. E. Durst, N. Nishimura, A. W. Wong, C. B. Schaffer, and C. Xu, Opt. Express **17**, 13354 (2009).
14. A. Aguirre, N. Nishizawa, J. Fujimoto, W. Seitz, M. Lederer, and D. Kopf, Opt. Express **14**, 1145 (2006).
15. Y. Deng and W. H. Knox, Opt. Lett. **29**, 2121 (2004).
16. Y. Yao, Y. Li, B. Liu, M. Hu, L. Chai, C. Wang, W. Tong, and J. Luo, Acta Opt. Sin. **28**, 1384 (2008).
17. M. Frosz, P. Falk, and O. Bang, Opt. Express **13**, 6181 (2005).
18. P. M. Moselund, M. H. Frosz, C. L. Thomsen, and O. Bang, Opt. Express **16**, 11954 (2008).
19. G. Genty, M. Lehtonen, H. Ludvigsen, and M. Kaivola, Opt. Express **12**, 3471 (2004).
20. W. Wang, H. Yang, P. Tang, C. Zhao, and J. Gao, Opt. Express **21**, 11215 (2013).
21. J. M. Dudley and J. R. Taylor, *Supercontinuum Generation in Optical Fibers* (Cambridge University, 2010).
22. F. Lu and W. H. Knox, Opt. Express **12**, 347 (2004).
23. J. W. Nicholson, A. D. Yablon, M. F. Yan, P. Wisk, R. Bise, D. J. Trevor, J. Alonzo, T. Stockert, J. Fleming, E. Monberg, F. Dimarcello, and J. Fini, Opt. Lett. **33**, 2038 (2008).